Received: 26 March 2021 | Revised: 11 November 2021 | Accepted: 16 November 2021

DOI: 10.1111/ijag.16546

INTERNATIONAL JOURNAL OF Applied Glass SCIENCE

RESEARCH ARTICLE

Femtosecond laser micromachining of integrated glass devices for high-order harmonic generation

Rebeca Martínez Vázquez[1] | **Anna G. Ciriolo**[1] | **Gabriele Crippa**[1,2] | **Valer Tosa**[3] | **Federico Sala**[1,2] | **Michele Devetta**[1] | **Caterina Vozzi**[1] | **Salvatore Stagira**[1,2] | **Roberto Osellame**[1,2]

[1] Institute for Photonics and Nanotechnologies (IFN), National Research Council (CNR), Milano, Italy

[2] Physics Department, Politecnico di Milano, Milano, Italy

[3] National Institute for R&D of Isotopic and Molecular Technologies, Cluj-Napoca, Romania

Correspondence
Rebeca Martínez Vázquez, Institute for Photonics and Nanotechnologies (IFN), National Research Council (CNR), Milano, Italy.
Email: rebeca.martinez@polimi.it

Funding information
ELI-RO_2020; _10 E03 Pulse-MeReAd; European Union's Horizon 2020 Research and Innovation program, Grant/Award Number: 964588; European Research Council Proof of Concept Grant FESTA, Grant/Award Number: 813103; Italian Ministry of Research and Education PRIN aSTAR 2017RKWTMY Consiglio Nazionale delle Ricerche Joint Laboratory ATTOBIO

Abstract

Femtosecond laser micromachining is a versatile technique that is broadly used for the fabrication of integrated optics and microfluidic devices. In this work, we present the fabrication and demonstration of a microfluidic device used for high-order harmonic generation in a hollow waveguide filled with helium. We found a higher generation yield and a harmonic spectrum reshaping (at gas baking pressures over 400 mbar) in the hollow waveguide with a smoother surface. We believe that, thanks to the high versatility and three-dimensional capability of this microstructuring technique, in the next future it will be possible to integrate more functionalities in the same glass chip thus paving the way to strong laser field physics in a lab-on-chip.

KEYWORDS

Femtosecond laser micromachining, Glass Hollow waveguides, High Order Harmonic Generation, Ultrafast laser sources

1 | INTRODUCTION

Femtosecond laser micromachining of dielectrics is an already established microfabrication technique that is continuously gaining interest, thanks to its high versatility and applicability in a broad spectrum of manufacturing fields. If compared to traditional methods, the main advantage of femtosecond laser processing is its capability of creating three-dimensional (3D) structures inside transparent materials at the micro and even nanometer scale, without the need for a cleanroom facility.[1,2]

When a femtosecond laser beam is focused inside a transparent material, nonlinear effects take place at the laser focus leading to a permanent and confined modification. In most dielectric materials, the physical and chemical properties of the irradiated region will depend on laser exposure conditions (pulse energy and focusing power), ranging from a local change in the material refractive index to embedded voids.[3,4] In particular, femtosecond laser irradiation followed by chemical etching (FLICE) is a technique that exploits the higher etching rate of the irradiated region, which is then selectively removed by

a suitable chemical etchant.[5,6] With this technique several microfluidic devices have been fabricated for applications ranging from chemistry to biology and materials science.[7–9]

Although microfluidic devices are typically dedicated to the manipulation of liquid samples, they are also suitable for the manipulation of gases, provided that they are perfectly sealed and made of a nonporous material. Indeed, there are examples in the literature of microfluidic chips dedicated to gas sensing.[10] Moreover, these empty structures buried inside glass can also be used as hollow waveguides that are particularly useful for high-field laser applications like spectral broadening, pulse compression, and high-order harmonic generation (HHG).[11–13]

When a strong laser field interacts with a neutral gas, highly nonlinear optical processes occur, among which the generation of high-order harmonics of the driving field. This process is associated with the up-conversion of the fundamental laser frequency in a broad spectrum of radiation, extending from the extreme ultraviolet (XUV) up to the soft-X ray spectral domain. Nowadays, the generation of XUV radiation by HHG is at the base of advanced spectroscopic techniques for probing ultrafast electron dynamics in atomic and molecular physics, and for the generation of attosecond pulses in time-resolved pump-probe measurements.[14–16] Since its demonstration,[17] the application of capillaries to HHG and attosecond pulse generation has attracted great interest.[13,18,19] If compared to more traditional generation approaches, based on gas-jets produced by pulsed valves, capillaries allow achieving both laser beam and gas confinement for a longer interaction length, thus leading to a dramatic increase of the generation yield. Moreover, capillaries can be filled with gas both in static and continuous-flow regimes, meaning that they are not subdued to technological limitations on repetition rate as pulsed valves and can be applied to high-repetition-rate lasers.

Unfortunately, the HHG and attosecond technology is not-yet fully accessible. Indeed, the generation of HHG radiation is limited to expensive and large laboratories that extend over several meter and are based on instrumentation that requires careful alignment and even active stabilization systems.[20] Moreover, the efficiency of HHG sources is extremely low, thus drastically hindering the possibility to attain a high photon flux, which is indeed a fundamental requirement for the study of low-density samples and low-efficiency processes, for example, pump-probe spectroscopy of molecules and transient absorption spectroscopy of materials.[21] In this framework, it is predictable that more efficient and miniaturized HHG sources will pave the way for their application in numerous novel fields.

In this work, we report on the application of the FLICE technique to the fabrication of integrated microfluidic glass devices devoted to XUV generation by HHG in helium gas. These devices are composed of a main microchannel that works as a hollow-core waveguide for the propagation of the femtosecond laser pulses at the fundamental frequency. The hollow waveguide is filled with gas using a microstructured network of delivery channels embedded in the same glass substrate and interfaced with the external gas pumps. High-order harmonics of the driving femtosecond laser field are generated within the waveguide by the interaction of the laser field with the gas. We optimized the optical guiding properties of the hollow waveguide; in particular, we investigate the effects of the internal surface quality on the propagation of the fundamental laser beam. Then, we measure the HHG spectra, evidencing its dependence on the waveguide surface roughness. We attribute this dependence to the interaction between the waveguide wall and the fundamental frequency laser beam, which could be considerably affected by scattering and absorption upon localized or distributed surface defects.

By allowing innovative engineering of the microfluidic structure and nanoscale-control of the surface quality, we believe that FLICE represents a powerful technology for the development of miniaturized devices for ultrafast photonics applications. Moreover, starting from these hollow-waveguide-based prototypes, we envisage the possibility to realize a new generation of lab-on-chip devices for HHG and attosecond science.

2 | MATERIALS AND METHODS

The devices are fabricated in fused silica glass substrates (UV grade fused silica, JGS1 from FOCtek) by the FLICE technique, which is intrinsically a two-step process. Initially, the glass sample is irradiated by a femtosecond laser. The irradiated volume is selectively removed with a subsequent chemical etching process.

For the irradiation of the glass samples, we used the setup schematically shown in Figure 1A. The laser source is a 1030 nm wavelength femtosecond laser from Amplitude Systems (Satsuma). It emits 230 fs laser pulses at a repetition rate ranging from 1 kHz to 40 MHz, with pulse energies up to 10 μJ. The laser beam passes through a 7-mm-long Lithium triborate (LBO) crystal that generates the second harmonic (515 nm). Afterward, the beam is focused inside the glass by a 63x (.65 numerical aperture) microscope objective (LD-plan Neofluor, Zeiss), equipped with a correction ring for spherical aberrations. The microscope objective and the sample are mounted onto 1D and 2D translation stages, respectively, with nanometer

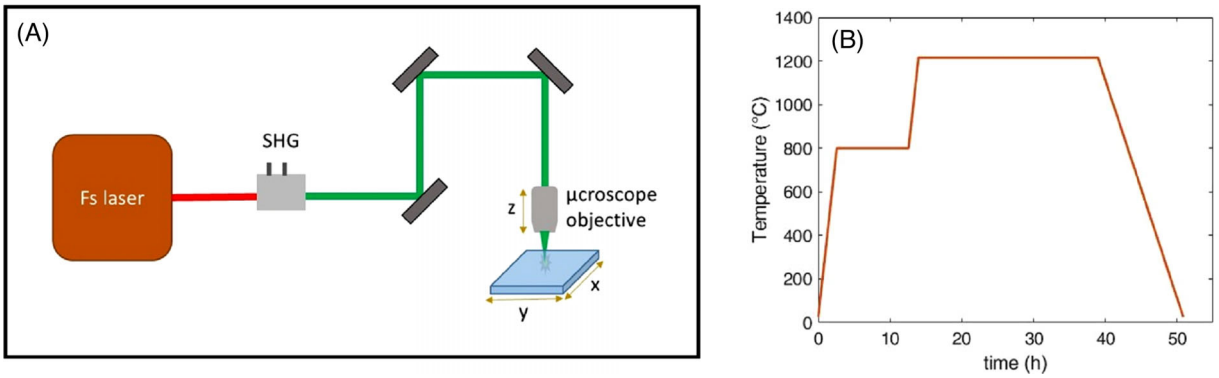

FIGURE 1 (A) Schematic view of the femtosecond laser micromachining setup; (B) annealing treatment to smooth fused silica microchannels

resolution (ANT130-035-L-ZS-PLUS and ANT95-50-XY-CMS-ULTRA, from Aerotech Inc.) allowing to create arbitrary 3D trajectories of the laser focus inside the sample. The laser beam is always polarized in the y-direction while the main translation direction is along x. For the fabrication of the HHG glass device the laser repetition rate is set to 1 MHz and the pulse energy to .3 μJ.

For the chemical etching, the samples are immersed in a 20% aqueous solution of hydrofluoric (HF) acid at 35°C in an ultrasonic bath. After etching, the glass device is accurately inspected by an optical microscope.

The hollow waveguide is fully characterized by the optical coupling of a laser at the same working wavelength as the one used for HHG. The optical characterization is performed outside the vacuum chamber. Here a 10 mW portion of the 800 nm laser beam of a femtosecond laser at 80 MHz, with a pulse duration lower than 100 fs (FemtoFiber pro NIR, Toptica), is focused on the waveguide entrance by a 20 cm focal-length lens. The sample is mounted on a four-axis nanometer movement stage (Nanomax, Thorlabs), which allows an accurate alignment to the impinging laser beam. The output mode of the waveguide is collected (near field) by a .3 numerical aperture aspheric objective lens (5725-B-H, Newport) and focused onto a charge-coupled-device camera (Spiricon). Particular attention was paid to avoid misalignments during output mode imaging. To measure the insertion losses, the camera is replaced by a power meter (Ophir).

The hollow waveguide surface smoothening[22] is performed with a furnace from Nabertherm (L5/13/P880). The sample is inserted into the heating chamber and subjected to the thermal treatment shown in Figure 1B. It is brought to the stress relief region of fused silica (1215°C) at a rate of 300°C/h. An intermediate step of 10 h at 800°C helps in evaporating contaminants present inside the heating chamber. The sample is then maintained at 1215°C for 25 h in order to ensure the smoothening of the entire channel, and cooled down until room temperature at a rate of 100°C/h.

The generation of high-order harmonics is performed by using ultrashort pulses (30 fs) with a central wavelength of 800 nm, produced by a multi-millijoule Ti:Sapphire laser source (Amplitude, Aurora laser system: 15 mJ, 30 fs pulses) working at a repetition rate of 1 kHz. A 500 μJ portion of the laser beam is focused at the entrance of the hollow waveguide by a 30 cm focal lens. The chip is mounted on a multiaxis actuator that allows an accurate adjustment of the position and the tilting angles. We optimize the coupling by looking at the far-field image of the output mode and maximizing the transmitted power of the 800 nm pulses through the waveguide, thus resulting in an average transmission higher than 80%.

HHG experiments are performed under a vacuum environment to prevent strong absorption of the generated XUV radiation by air. For this reason, the chip is installed in a vacuum chamber, which is constantly kept at 10^{-5} mbar by a vacuum pump system.

The device is directly connected to a pipeline, through which the gas flows from outside to inside the vacuum chamber. Upstream the gas distribution pipe a needle valve and a capacitive pressure gauge allow accurate control of the gas backing pressure. In this experiment we used backing pressures up to 1 bar; this limit is imposed by the pumping system, but higher pressures can be in principle applied to the device.

The HHG signal produced inside the chip is detected by a grazing incidence spectrometer working in stigmatic configuration. A more detailed description of the experimental setup used for the generation and the acquisition of the HHG spectra is provided in a previous work.[13]

To reveal the details of harmonic generation in cylindrical hollow waveguides, we performed a theoretical analysis using a nonadiabatic 3D model for the propagation of both driving laser pulse and generated harmonic field.[23]

The propagation of the driving laser pulse is simulated by solving the 3D wave equation with cylindrical symmetry, including effects of dispersion, absorption, third-order nonlinearities, and ionization. For the harmonic field calculation, the single-atom response was obtained using the strong field approximation[14] and 3D propagation was simulated with the source term calculated from the single-atom response. The propagation equation for the driving field was solved exploiting the operator-splitting method. We first solve its homogeneous part by projecting the field onto the eigenmodes whose propagation and mode loss constants are known.[24] By writing the field as a superposition of the eigenmodes we also fulfil the boundary conditions of the hollow waveguide. The nonlinear part of the propagation equation takes the form of an ordinary differential equation that can be solved by standard methods.

In the calculations, we assume that the spatial distributions of the driving field at the entrance of the hollow waveguide is the lowest EH_{11} mode.[24] This assumption is valid as long as the ratio between the beam waist of the incident laser and the radius of the waveguide is about 65%.[25]

3 | RESULTS AND DISCUSSION

3.1 | The architecture of the glass device for HHG

The external shape of the HHG glass device is of a rectangular parallelepiped with dimensions of 8 mm length, 10 mm width, and 1 mm thickness. It contains the microchannel network that is made of a top rectangular inlet connected to the main channel (hollow waveguide) through four micrometer-sized vertical channels (see Figure 2A).

The FLICE technique allows for the fabrication of buried microchannels with extremely fine control on geometry, shape, and size. To achieve such control, the irradiation trajectory must be accurately studied to compensate for several additional effects undergoing during the etching process, including the etching of nonirradiated material whenever exposed to HF, and the etching rate dependence on the laser polarization. Namely, the etching rate is maximum (~1 mm/h) when the laser polarization is perpendicular to sample translation.[26] The irradiation of the microfluidic network is made in a bottom–top direction (first the hollow waveguide, then the micrometer-sized vertical channels and finally the top rectangular inlet), with the microscope objective correcting ring fixed at the hollow waveguide depth position (~350 μm).

Each component is irradiated following a dedicated irradiation path depending on their geometry, position, and exposure timing to the etchant bathing. To fabricate the hollow waveguide we adopted a multiscan irradiation approach, that consists of irradiating the sample through contiguous straight lines (8 mm length) with a separation between them of 1 μm, following the surface of a cylinder (see Figure 2A). The cross-section of the irradiated cylinder is elliptically shaped: this allowed to compensate for the spherical aberration along laser beam propagation direction, thus obtaining a circular section after etching.[27] The gas-delivery channels were made by irradiating single vertical lines from the top of the hollow waveguide until the base of the reservoir. We added two more auxiliary vertical channels in order to allow a subsequent homogeneous etching of the hollow waveguide. The shallow rectangular inlet is made by the multiscan approach (1 μm separation between scans) irradiating the base and lateral walls of a rectangular parallelepiped with dimensions of 2 mm length x 4.7 mm width x .1 mm thickness.

The translation speeds were 2 mm/s for the hollow waveguide, .3 mm/s for the vertical channels, and 5 mm/s for the rectangular inlet.

After the irradiation, the sample is immersed in a 20% HF solution for 2 h 30 min, under sonication. Figure 2B,C shows, respectively, a picture of the overall device and the microscope images of the hollow waveguide region after the etching process.

The top rectangular chamber is exposed to the etchant solution before the inner components (hollow waveguide and gas-delivery channel). As a result, it also serves as a chamber for etchant harvesting and uniform distribution at the entrance of the vertical microchannels. After etching we obtained vertical channels shaped as 100-μm-long cylinders with a slightly different top-to-bottom diameter (from 50 to 40 μm diameter). These channels are equally spaced along the waveguide direction, with a relative distance $\Delta x = 1.2$ mm. This pattern of vertical channels has two major advantages. First, it ensures the etchant to synchronously attack the waveguide glass from multiple and evenly distributed sites, thus leading to a hollow waveguide with a uniform diameter (130 μm) within the whole 8 mm chip length.[13] Moreover, the multiple-channels arrangement is of crucial importance for HHG since it makes possible to achieve an almost uniform gas density distribution inside the hollow waveguide.

3.2 | Surface roughness

The propagation of ultrashort pulses in these devices is directly determined by the optical properties of the hollow-core waveguide. In this sense, the optical quality of the capillary surface provides a crucial issue for HHG applications. Indeed, it is known that the surface irregularities

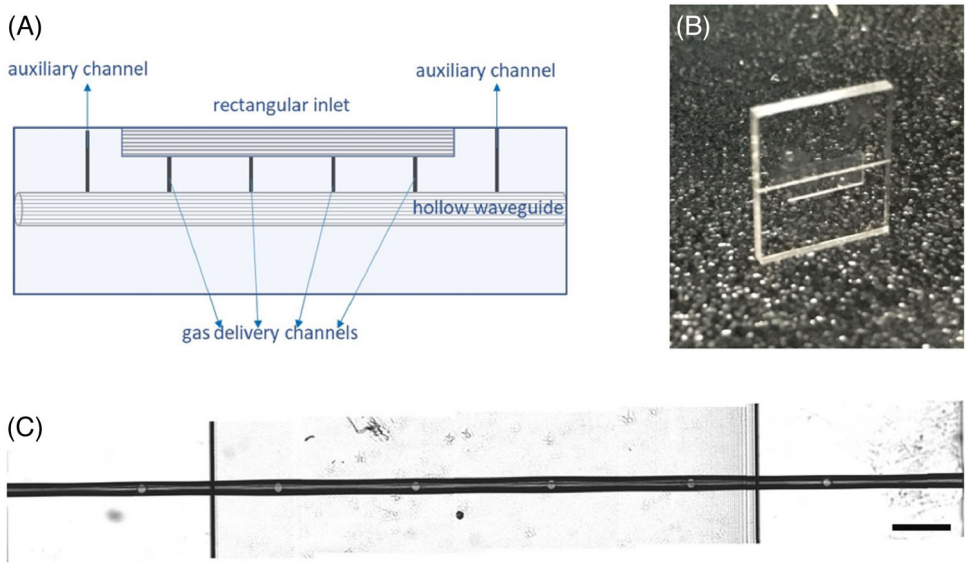

FIGURE 2 (A) Two-dimensional scheme (not in scale) of the irradiated components for the device fabrication; (B) picture of the glass chip after laser irradiation and hydrofluoric (HF) etching; (C) microscope image, from top, of the hollow waveguide region after the etching step, scale bar: 500 μm

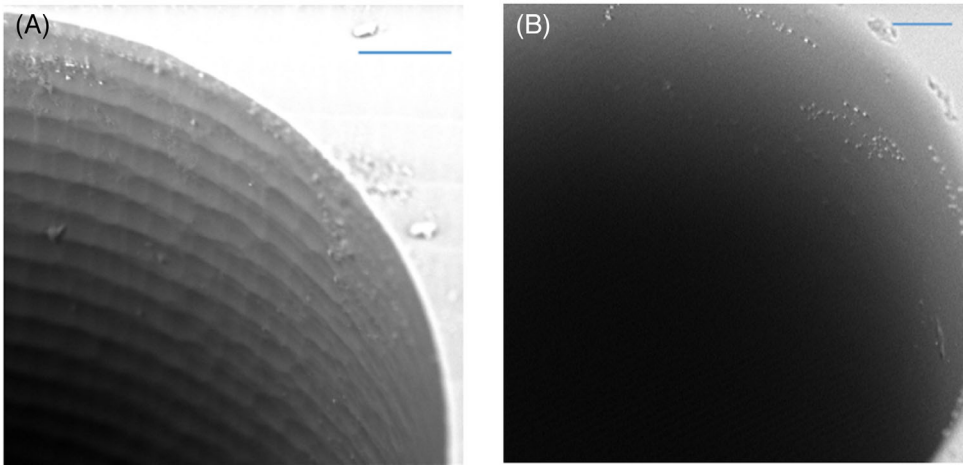

FIGURE 3 Scanning electron microscope (SEM) image of waveguide inner surface before (A) and after (B) the thermal annealing. Scale bars: 10 μm

in hollow waveguides influence the propagation of visible/infrared radiation by introducing extra losses.[28] However, to our knowledge, there are no studies in the literature exploring the role of surface quality on the generation and propagation of XUV radiation.

To this purpose, we investigate the difference, in terms of HHG yield, of two devices characterized by the same internal structure, one with the typical surface roughness resulting from the etching process and one smoothened by a thermal process (see Figure 3). After the etching process, the hollow waveguide surface presents a ripple pattern due to the scanning step, made of parallel grooves with a 5 μm periodicity (see Figure 3A). With isothermal annealing (see details in Section 2), the hollow waveguide surface roughness is highly improved as could be seen by scanning electron microscope (SEM) images presented in Figure 3A,B. We did not measure the final roughness of the channels but from many previous results present in the literature[11,22] we estimate that it is reduced to a few nanometers.

We characterized the optical properties of the waveguide before and after the annealing using the setup described in Section 2. The near field images of the output beam (see Figure 4) show that it is made by a single mode in both cases with profiles matching a zero-order Bessel function, as expected from a hybrid mode EH_{11}.[24] The mode of the annealed waveguide (~50 μm) is slightly larger than that of the not annealed one (~40 μm); this is an unexpected

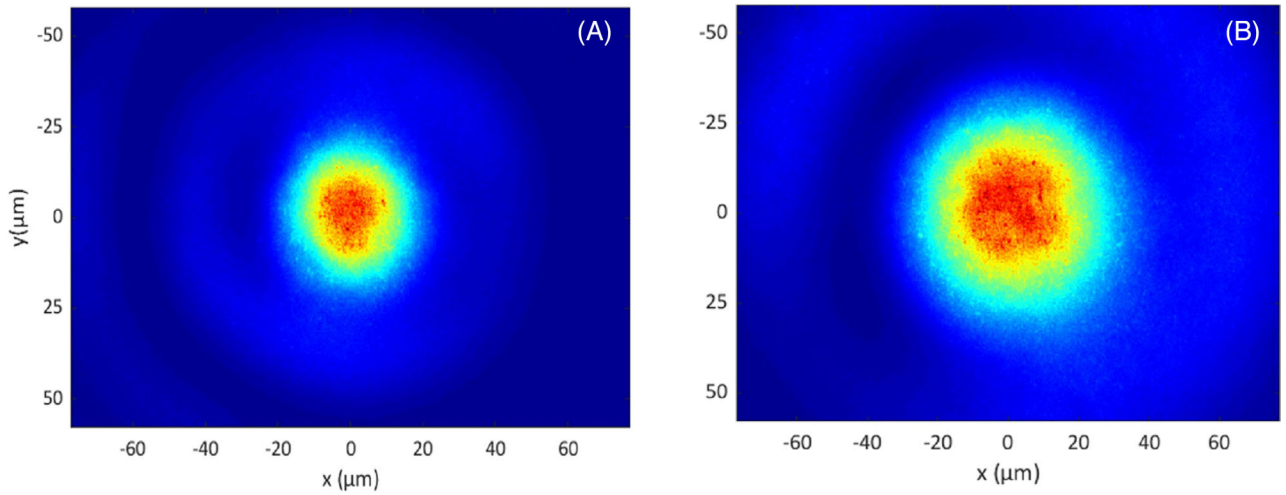

FIGURE 4 Coupled mode image of the hollow waveguide before (A) and after (B) the thermal annealing

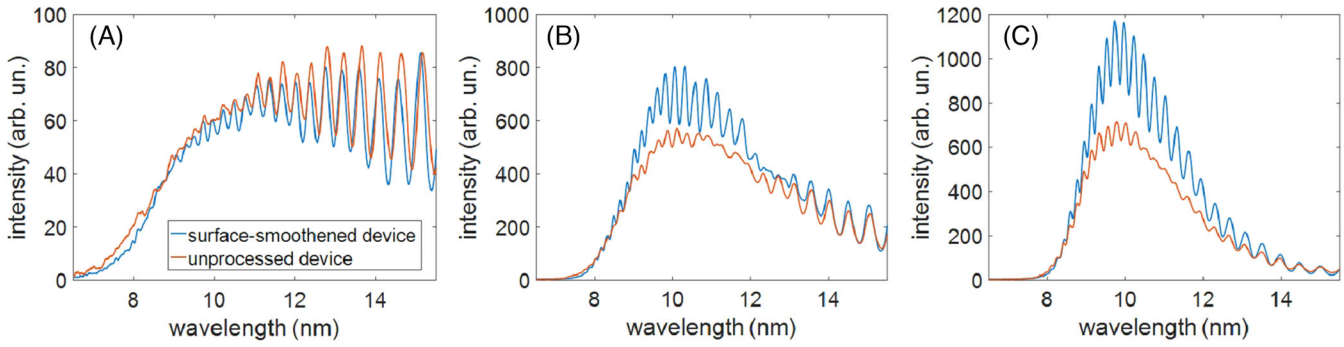

FIGURE 5 High-order harmonic spectra generated inside the glass chips filled with helium at different backing pressures: 100 mbar (A), 400 mbar (b), and 1 bar (C). Red spectra are obtained by using a thermally unprocessed device, blue spectra are instead obtained from a surface-smoothened device after baking treatment

behavior since by inspection at the optical microscope image we do not see a macroscopic increase in the waveguide diameter after annealing. Therefore, we attribute the difference between the two mode profiles to the surface roughness, which could affect the mode transverse distribution (or even induce the propagation of different waveguide modes).

The waveguide insertion losses remain stable at a value of .8 dB even after the surface smoothing. Most probably, the waveguides are too short to see a considerable difference in the propagation losses due to surface roughness.

3.3 | Generation of high-order harmonics in the FLICE devices

Figure 5 shows the comparison between harmonics spectra generated inside chips endowed with different surface quality. Helium was used as an interaction medium at different backing pressures. HHG spectra are all characterized by a typical fringe pattern corresponding to the odd harmonics of the fundamental driving frequency, extending below 7 nm wavelength.

At low pressure (100 mbar), the HHG spectra exhibit a large spectral bandwidth, with well-defined harmonics at longer wavelengths and an almost continuum spectrum at the spectral cut-off (below 9 nm). In this pressure condition, the XUV generated inside the two devices is comparable, both in terms of yield and shape.

By increasing the pressure, the yield of the XUV spectrum shows an enhancement. The increase in the generation efficiency is related to the higher number of atoms involved in the emission process but it is nonuniform along the spectrum. In particular, an enhancement appears at 10 nm, while long-wavelength components are less affected by pressure changes. At both 400 mbar and 1 bar, a considerably higher yield can be achieved in the device with a smoothed internal surface. Moreover, the

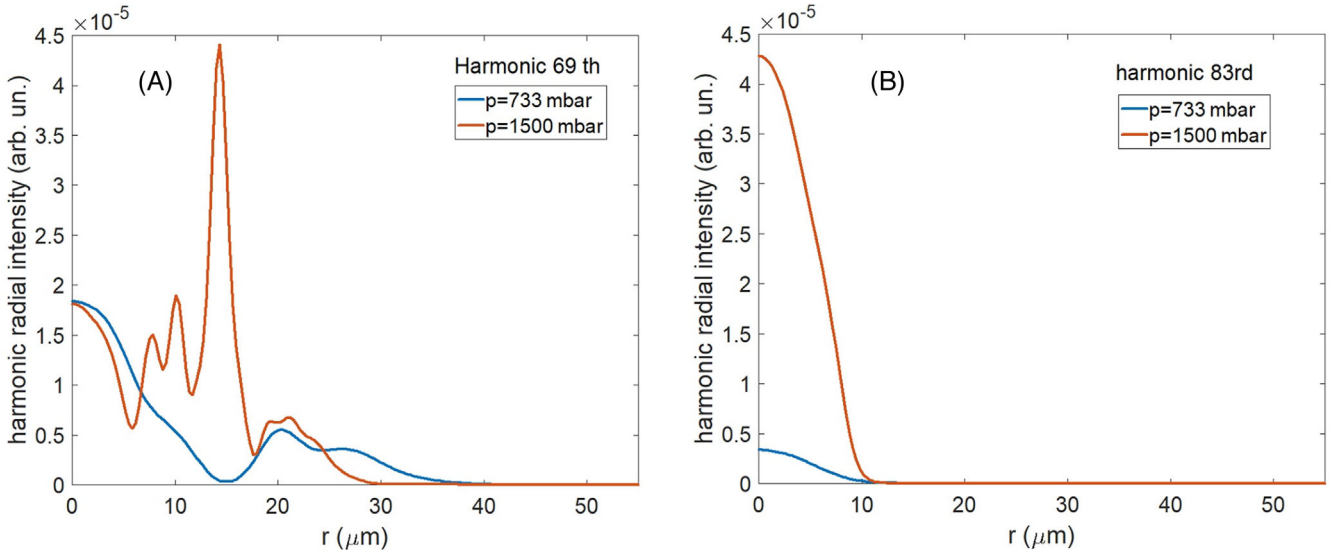

FIGURE 6 Simulated radial intensities at the waveguide exit for two harmonics (H69 (A) and H83 (B)) at two different helium pressures (733 mbar (A) and 1500 mbar (B)). The harmonic distribution is calculated up to the diameter of the waveguide ($r = 65\ \mu$m), but, for sake of clearness, here we show a radial axis from 0 to 55 μm

higher the pressure the larger the discrepancy between the generation efficiencies in the two cases.

Another interesting effect is that the harmonics spectrum undergoes a reshaping depending on the gas backing pressure, which noticeably depends on the specific device. The modulation of the spectrum as a function of the gas pressure is due to the interplay of absorption and de-coherence effects undergoing in an extended generation medium, composed of a collection of emitters with a nonuniform phase. The differences observed in the two devices emphasize the role of structural properties, such as the surface roughness of hollow-core waveguide, which are still mostly unexplored.

To investigate the propagation of the XUV radiation, we performed numerical calculations of HHG in the 8-mm-long cylindrical hollow waveguide filled with He gas, and made a detailed analysis of harmonics in the spectral region where we have experimentally found the higher increase in generation efficiency between the two devices. As described in Section 2, the propagation of the driving laser pulse and the generation of the XUV was carried out by solving the 3D wave equation with cylindrical symmetry and the single-atom response in a strong field approximation, respectively. The gas density used in the model was determined by using the High-Mach Number Flow Model of Comsol Multiphysics.[13] Despite the numerical model relies on the assumption of an ideal dielectric hollow-core waveguide, the radial extension of the harmonic field can give inspection into the role of the surface and its defects on the generation and propagation of the XUV field. Indeed, we expect that the larger is the radial profile of harmonics, the more they are affected by interaction with the interface.

Figure 6 reports the numerical radial intensities of two spectral components in the region of interest, at two different gas pressures. In particular, the figure shows the 69th (~11 nm) and 83rd (~9 nm) harmonics intensities, at the waveguide exit, as a function of the radial coordinate. At lower pressure (733 mbar), the two harmonics intensities are strongly confined within a small radial volume and exhibit the main intensity peaks nearly in the center of the waveguide. The 69th component exhibits an out-of-axis contribution, which becomes more intense at higher pressure (1500 mbar) resulting in a strong peak at $r = 14\ \mu$m, which is however too far from the waveguide surface (at $r = 65\ \mu$m). In our conditions, the numerical results show strong confinement of the harmonics field, both on the on-axis and off-axis components, thus suggesting a negligible harmonic-to-surface interaction.

Based on these computational results, we believe that the dependence of HHG on the waveguide surface quality cannot be directly attributed to surface effects on the generated XUV. However, by referring to Figure 4, we see that the fundamental field is strongly influenced by the glass surfaces (a remarkable resizing of the waveguide mode occurs depending on the wall roughness) which indirectly affects the generation yield. Since HHG is a strongly nonlinear process, it provides particularly sensitivity to any external factor affecting the fundamental laser field intensity and shape.

Thus, the optical quality and profile of the waveguide walls play a crucial role, remarkably affecting the generation performances of the glass devices for on-chip HHG. We foresee that an accurate engineering of the interfaces will be possible by properly calibrating the irradiation and

thermal treatment parameters, thus allowing the fabrication of glass devices with enhanced performances.

4 | CONCLUSIONS

Femtosecond laser micromachining is a suitable technique for the fabrication of glass microfluidic devices devoted to the interaction between ultrafast laser beams and gases for XUV radiation generation. The combination of miniaturized HHG beamlines together with an increased generation efficiency will potentially allow a spread of these facilities to unexpected new research fields. This study explores the fabrication by FLICE technique of a few millimeter-sized glass devices for the manipulation of helium gas and confinement of a femtosecond laser beam in a hollow waveguide. The interaction inside the hollow waveguide between gas and the laser beam leads to the generation of high-order harmonics. We observed a remarkable generation yield improvement in a thermally treated device, which states the importance of hollow waveguide surface roughness in this highly nonlinear regime. These results demonstrate the possibility of exploiting the 3D intrinsically capability of FLICE to realize more complicated integrated devices, for a future XUV and attosecond science in a chip.

AUTHOR CONTRIBUTIONS

Conceptualization: Anna G. Ciriolo, Caterina Vozzi, Rebeca Martínez Vázquez, Roberto Osellame, and Salvatore Stagira. *Formal analysis*: Rebeca Martínez Vázquez, Anna G. Ciriolo, and Valer Tosa. *Funding acquisition*: Caterina Vozzi, Michele Devetta, Roberto Osellame, Rebeca Martínez Vázquez, Salvatore Stagira, and Valer Tosa. *Investigation*: Anna G. Ciriolo, Gabriele Crippa, Michele Devetta, Rebeca Martínez Vázquez, and Valer Tosa. *Methodology*: Anna G. Ciriolo, Caterina Vozzi, and Rebeca Martínez Vázquez. *Validation and writing—original draft*: Anna G. Ciriolo and Rebeca Martínez Vázquez. *Writing—review and editing*: all authors.

ACKNOWLEDGMENTS

Valer Tosa acknowledge partial funding from project ELI-RO_2020_10 E03 Pulse-MeReAd. This project has received funding from the European Union's Horizon 2020 Research and Innovation program under grant agreement no. 964588 (XPIC). This study was partially supported by the European Research Council Proof of Concept Grant FESTA (grant no. 813103), by the Italian Ministry of Research and Education with the projects ELI–ESFRI Roadmap and PRIN aSTAR (2017RKWTMY), by the Consiglio Nazionale delle Ricerche with the Joint Laboratory ATTOBIO.

ORCID

Rebeca Martínez Vázquez https://orcid.org/0000-0001-8728-5819

REFERENCES

1. Gattass RR, Mazur E. Femtosecond laser micromachining in transparent materials. Nat Photonics. 2008;2:219–25.
2. Xu BB, Zhang YL, Xia H, Dong WF, Ding H, Sun H. B. Fabrication and multifunction integration of microfluidic chips by femtosecond laser direct writing. Lab Chip. 2013;13:1677–90.
3. Davis KM, Miura K, Sugimoto N, Hirao K. Writing waveguides in glass with a femtosecond laser. Opt Lett. 1996;21:1729–31.
4. Glezer EN, Milosavljevic M, Huang L, Finlay RJ, Her TH, Callan JP, et al. Three-dimensional optical storage inside transparent materials. Opt Lett. 1996;21:2023–5.
5. Marcinkevicius A, Juodkazis S, Watanabe M, Miwa M, Matsuo S, Misawa H, et al. Femtosecond laser-assisted three-dimensional microfabrication in silica. Opt Lett. 2001;26:277–9.
6. Masuda M, Sugioka K, Cheng Y, Aoki N, Kawachi M, Shihoyama K, et al. 3-D microstructuring inside photosensitive glass by femtosecond laser excitation. Appl Phys A: Mater Sci Process. 2003;76:857–60.
7. Osellame R, Hoekstra HJ, Cerullo G, Pollnau M. Femtosecond laser microstructuring: an enabling tool for optofluidic lab-on-chips. Laser Photon Rev. 2011;5:442–63.
8. Sima F, Sugioka K, Martínez Vázquez R, Osellame R, Kelemen L, Ormos P. Three-dimensional femtosecond laser processing for lab-on-a-chip applications. Nanophotonics 2018;7:613–34.
9. Vitali, V, Nava G, Zanchetta G, Bragheri F, Crespi A, Osellame R, et al. Integrated optofluidic chip for oscillatory microrheology. Sci Rep. 2020;10:5831
10. Rebordão G, Palma SICJ, Roque ACA. Microfluidics in gas sensing and artificial olfaction. Sensors 2020;20(20):5742.
11. He F, Lin J, Cheng Y. Fabrication of hollow optical waveguides in fused silica by three-dimensional femtosecond laser micromachining. Appl Phys B. 2011;105:379–84.
12. Cirirolo AG, Martínez Vázquez R, Roversi A, Frezzotti A, Vozzi C, Osellame R, et al. Femtosecond laser-micromachining of glass micro chip for high order harmonic generation in gases. Micromachines 2020;11:165.
13. Ciriolo AG, Martínez Vázquez R, Tosa V, Frezzotti A, Crippa G, Devetta M, et al. High-order harmonic generation in a microfluidic glass device. J Phys Photonics. 2020;2:024005.
14. Lewenstein M, Balcou PH, Ivanov MY, L'Huillier A, Corkum PB. Theory of high-harmonic generation by low-frequency laser fields. Phys Rev A. 1994;49:2117–32.
15. Krausz F, Ivanov M. Attosecond physics. Rev Mod Phys. 2009;81:163–234.
16. Calegari F, Sansone G, Stagira S, Vozzi C, Nisoli M. Advances in attosecond science. J Phys B: At Mol Opt Phys. 2016;49:062001.
17. Durfee CG, Backus S, Murnane MM, Kapteyn HC. Ultrabroadband phase-matched optical parametric generation in the ultraviolet by use of guided waves. Opt Lett. 1997;22:1565–7.
18. Popmintchev T, Chen M-C, Bahabad A, Gerrity M, Sidorenko P, Cohen O, et al. Phase matching of high harmonic generation in

the soft and hard X-ray regions of the spectrum. Proc Nat Acad Sci USA. 2009;106(26):10516–21.
19. Ackermann P, Laforgue X, Hilbig M, Schilder M, Halfmann T. Phase-matched harmonic generation in gas-filled waveguides in the vicinity of a multiphoton resonance. J Opt Soc Am B. 2018;35:468–80.
20. Kühn S, Dumergue M, Kahaly S, Mondal S, Füle M, Csizmadia T, et al. The ELI-ALPS facility: the next generation of attosecond sources J Phys B: At Mol Opt Phys. 2017;50:132002.
21. Young L, Ueda K, Gühr M, Bucksbaum PH, Simon M, Mukamel S, et al. Roadmap of ultrafast X-ray atomic and molecular physics J Phys B: At Mol Opt Phys. 2018;51:032003 .
22. Sala F, Paié P, Martínez Vázquez R, Osellame R, Bragheri F. Effects of thermal annealing on femtosecond laser micromachined glass surfaces. Micromachines 2021;12(2):180.
23. Tosa V, Kim HT, Kim IJ, Nam CH. High-order harmonic generation by chirped and self-guided femtosecond laser pulses. I. Spatial and spectral analysis Phys Rev A. 2005;71:063807.
24. Marcatili EAJ, Schmeltzer RA. Hollow metallic and dielectric waveguides for long distance optical transmission and lasers. Bell Syst Techn J. 1964;43(4):1783–809.
25. Nisoli M, Stagira S, De Silvestri S, Svelto O, Sartania S, Cheng Z, et al. A novel-high energy pulse compression system: generation of multigigawatt sub-5-fs pulses. Appl Phys B: Lasers Opt. 1997;65:189–96
26. Vishnubhatla KC, Bellini N, Ramponi R, Cerullo G, Osellame R. Shape control of microchannels fabricated in fused silica by femtosecond laser irradiation and chemical etching. Opt Express. 2009;17:8685–95.
27. Marcinkevičius A, Mizeikis V, Juodkazis S, Matsuo S, Misawa H. Effect of refractive index-mismatch on laser microfabrication in silica glass. Appl Phys A. 2003;76(2):257–60.
28. Matsuura Y, Saito M, Miyagi M, Hongo A. Loss characteristics of circular hollow waveguides for incoherent infrared light. J Opt Soc Am A. 1989;6(3):423–7.

How to cite this article: Martínez Vázquez R, Ciriolo AG, Crippa G, Tosa V, Sala F, Devetta M, et al. Femtosecond laser micromachining of integrated glass devices for high-order harmonic generation. Int J Appl Glass Sci. 2022;13:162–170. https://doi.org/10.1111/ijag.16546